Supplementary Information

Length-Dependent Thermopower of Highly Conducting Au-C Bonded Single Molecule Junctions

J. R. Widawsky[1], W. Chen[3], H. Vazquez[1], T. Kim[1,3], R. Breslow[3], M. S. Hybertsen*[2], L. Venkataraman*[1]

[1]*Department of Applied Physics and Applied Mathematics, Columbia University, New York, NY*

[2]*Center For Functional Nanomaterials, Brookhaven National Laboratory, Upton, NY*

[3]*Department of Chemistry, Columbia University, New York, NY*

*AUTHOR EMAIL ADDRESS: lv2117@columbia.edu, mhyberts@bnl.gov

Contents:

Measurement, Data Analysis and Additional Data:

The following molecules were synthesized according to procedures previously reported in literature[1, 2] and used for the measurements reported here. All structures are shown in SI Figure S1:

1) 1,4-bis((trimethylstannyl)methyl)benzene (**P1**)
2) 4,4'-bis((trimethylstannyl)methyl)-1,1'-biphenyl (**P2**)
3) 4,4''-bis((trimethylstannyl)methyl)-1,1':4',1''-terphenyl (**P3**)
4) 4,4'''-bis((trimethylstannyl)methyl)-1,1':4',1'':4'',1'''-quaterphenyl (**P4**)
5) 1,6-Bis(trimethylstannyl)hexane (**C6**)
6) 1,6-Bis(trimethylstannyl)octane (**C8**)
7) 1,10-Bis(trimethylstannyl)decane (**C10**)

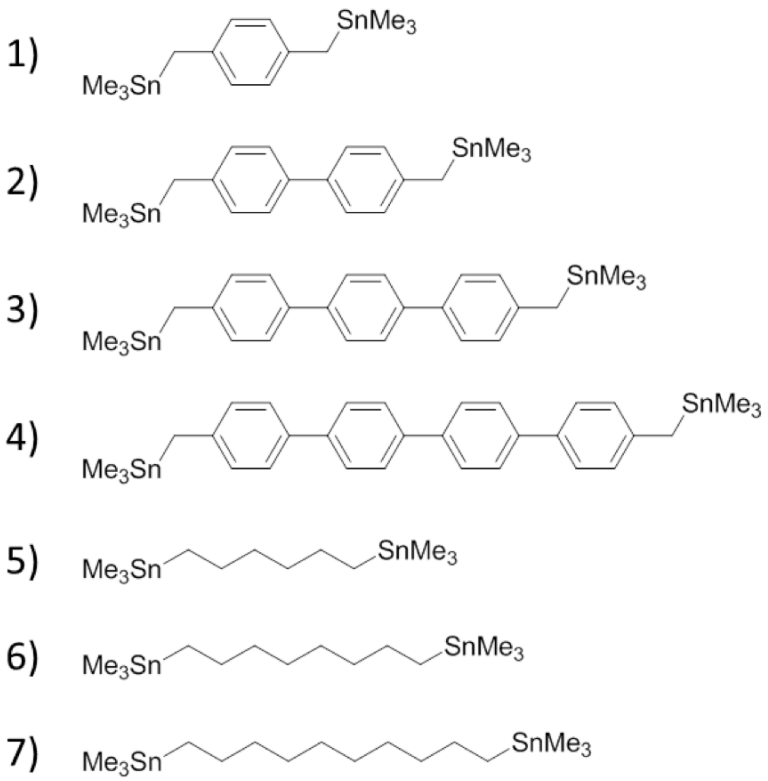

SI Figure S1: Structures of the molecules used in the STM-BJ experiment. The trimethyltin end groups cleave off both sides in situ allowing the terminal carbons to covalently bind to the gold electrodes.

The conductance of each molecule was measured using the STM-based break-junction technique[3, 4], where an Au tip (Alfa Aesar, 99.998%) cut to be sharp is brought in and out of contact with a substrate

of ~100 nm of gold (Alfa Aesar, 99.999%) evaporated onto cleaved mica disks. The substrate is mounted on a piezoelectric positioner (Mad City Labs), so that sub-angstrom resolution in position is achieved. During the entire break junction procedure, a small, constant bias (10 mV) is applied between the tip and the substrate with a 10kΩ series resistance added in the circuit while the current is measured (Keithley 428-Prog). Piezo control and data collection were performed using a National Instruments PXI Chassis System (with PXI-4461, PXI-6289) at 40 kHz and driven and managed with a custom-program using Igor Pro (Wavemetrics, Inc.). The experimental set-up is kept under ambient conditions.

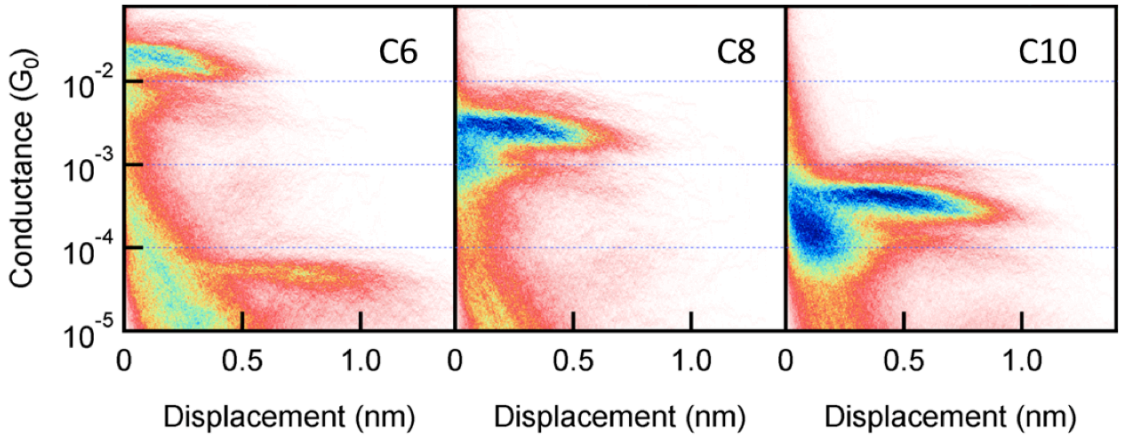

SI Figure S2: Two-dimensional conductance histograms of C6, C8, and C10. Thousands of conductance traces are aligned at the rupture of the gold point contact to generate the 2D histograms. The bins have a width of 0.008 nm along the displacement axis and 100/decade along the conductance axis. The feature between 10^{-5} and 10^{-4} G_0 in the 2D histogram for C6 is due to the in situ formation of the dimer molecule, C12.

For each experiment, the substrate is cleaned under UV/Ozone for 15 minutes prior to use. For every conductance trace measurement, the STM tip is first brought into hard contact with the substrate to achieve a conductance greater than ~ 10 G0. At this point, the junction electrodes are pulled apart at a speed of 16 nm/s for 250 ms. Conductance is measured as a function of tip-sample displacement to generate conductance traces. For each tip/substrate pair, at least one set of 1,000 traces of clean gold breaks is collected first to ensure the system is clean. Then, the target molecule is dissolved in acetone (~10mM) and drop cast onto the substrate. The solvent is allowed to evaporate so that a dry layer of analyte remains and an additional 1,000 conductance traces are collected before starting the thermoelectric current measurement.

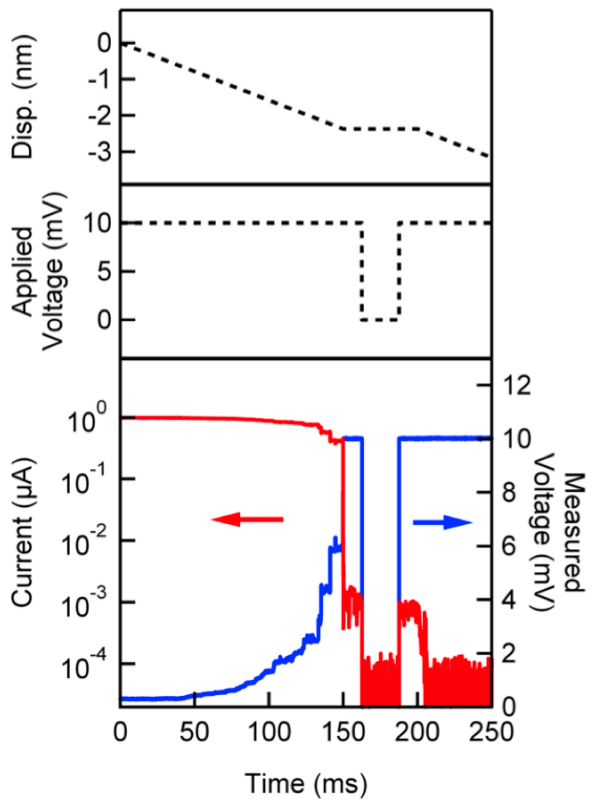

SI Figure S3: Top: Piezo ramp used, including a "hold" portion between 150 and 200 ms. Middle: External applied voltage across the leads which drops to zero during the center of the "hold" portion. Bottom: Sample trace for molecular junction. The measured current is shown in red and the voltage measured across the junction is shown in blue.

For measurement of thermoelectric current, the preceding procedure was modified[5]. A "hold" portion was incorporated into the piezo pull-out ramp, where after the piezo stretched the junction for 2.37 nm, the junction was held constant for 50 ms, and then the stretching continued until the junction was broken. During the central two quartiles of the hold (middle 25 ms), the applied bias was dropped to zero, so that all of the current measured would be due solely to the thermal gradient. The electronics was carefully calibrated to ensure that there were no other sources of bias across the junction after every 50 measurements. The substrate was mounted onto the hot side of a thermoelectric (Peltier) device, while the cold side was kept near room temperature. Additionally, the STM tip was kept near room temperature throughout the measurement. The temperature of the hot substrate and the tip was recorded using a thermocouple. For each molecule, more than a few thousand thermal current traces were collected at each ΔT's (0 K and ~14 K), though not every trace included a molecular junction during the "hold" period (i.e. if the gold point contact ruptured "too early" or "too late"). To determine if a molecule was held during this period, the average conductance of the first and fourth quartiles of the

hold (i.e. when the applied bias was 10 mV) was analyzed. If it was within the conductance peak of that respective molecule then the trace was selected. A schematic depiction of the procedure along with a sample trace is given in SI Figure S3.

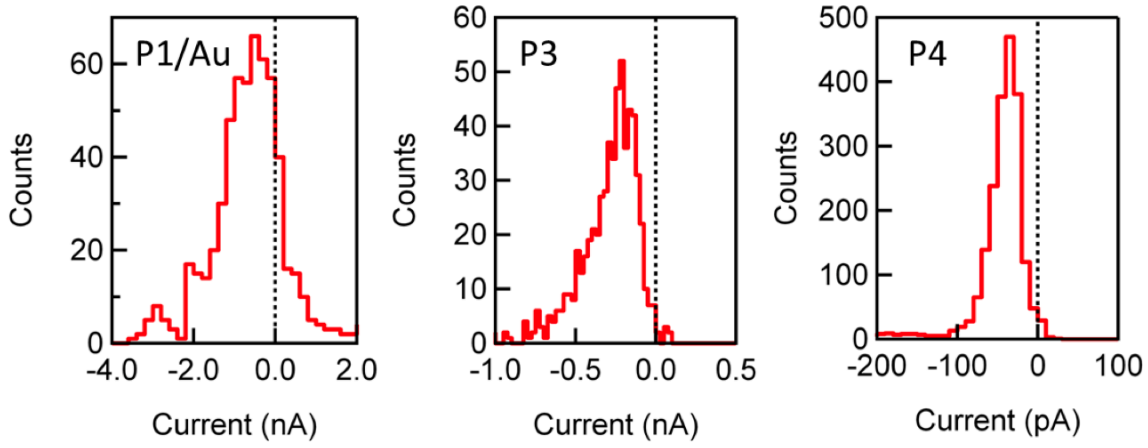

SI Figure S4: Average thermoelectric current histograms for P1/Au (582 traces), P3 (629 traces), and P4 (2,942 traces) for $\Delta T \sim 14$ K. The thermoelectric current histograms for each at $\Delta T = 0$ K (not shown) are narrow and centered at 0 nA and are represented here by dotted lines.

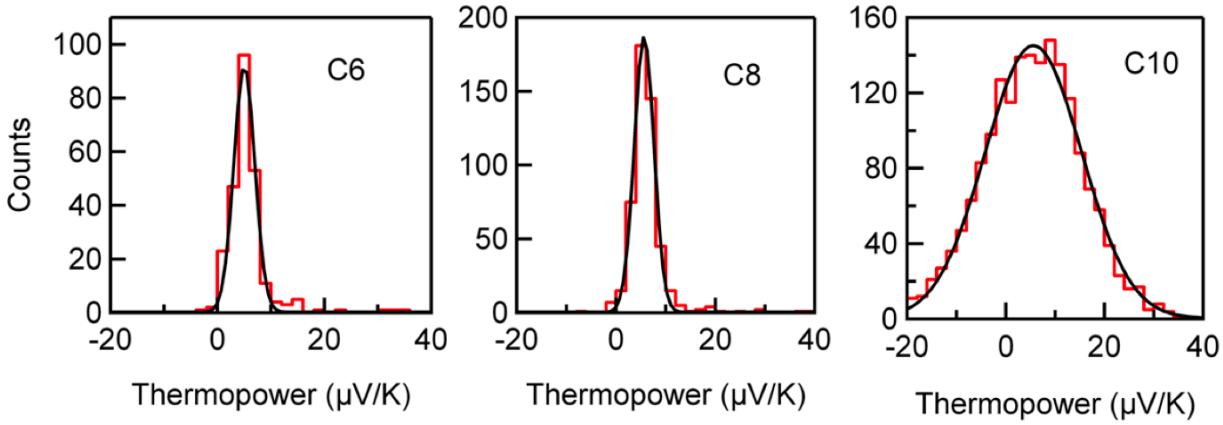

SI Figure S5: Histograms of thermopower for C6 (250 traces), C8 (506 traces), and C10 (1,815 traces). The histograms are fit with Gaussians to determine the most frequently measured molecular junction thermopower. The peak thermopower for all three alkanes is 5.0-5.6 μV/K. The width of the C10 distribution is attributed to signal to noise limitations.

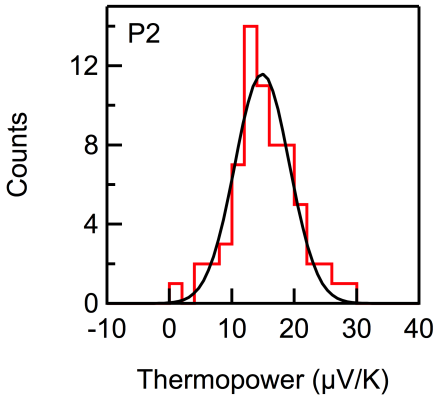

*SI Figure S6: Histograms of thermopower for **P2** measured with a $\Delta T \sim 25$ K. The histogram is fit with Gaussians to determine the most frequently measured molecular junction thermopower. The peak thermopower is 14 μ V/K.*

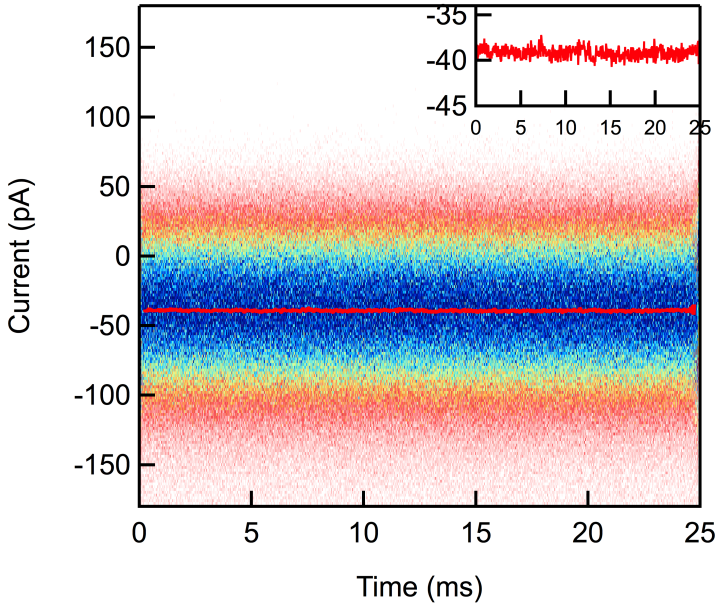

*SI Figure S7: Current as a function of hold time for all **P4** junctions measured shown as a two-dimensional histogram. The current does not change as a function of hold-time indicating that the temperature difference across the junction does not change with time. Inset shows a zoom in of the average current as a function of time determined by fitting sections of the two-dimensional histograms with Gaussians and obtaining the peak value.*

Alternative Models:

Single-Lorentzian Results: We start with the single-Lorentzian model for which the conductance and thermopower are used to determine the energy level alignment relative to the Fermi energy $E_F - E_0$ and the coupling Γ from the equations below[5, 6]:

$$\mathrm{T}(E) = \frac{\Gamma^2/4}{(E_0 - E)^2 + \Gamma^2/4}; \quad E_F - E_0 = 2\frac{S_0}{S}\left(1 - \frac{G}{G_0}\right); \quad \Gamma = \sqrt{\frac{8GS_0(E_F - E_0)}{SG_0}}$$

where S_0 = 7.2576 eV × 1μV/K and G_0 = 77.5 μS. The data in Table 1 are used to generate the Lorentzian transmission curves given in SI Figure S8.

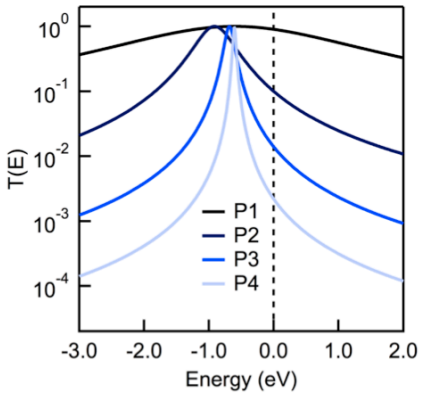

SI Figure S8: Lorentzian transmission functions determined individually for each of the oligophenyls measured using the measured values of conductance and thermopower following the equations given above.

Modeling Transmission and Fitting Data: For all tight-binding models we first determine the Hamiltonian matrix. The retarded Green's function for the model junction is then $G(E) = [E\mathbb{I} - H]^{-1}$ and the transmission is given by $\mathcal{T}(E) = \Gamma^2|G_{LR}|^2$ where G_{LR} denotes the component of the Green's function matrix that describes the propagation between the left and right electrodes[7]. From this, the conductance and thermopower are calculated numerically. We use this to determine the best fit-coefficients for our data as follows. We pick a set of coefficients, calculate the transmission functions for all molecules and determine all conductances and thermopowers at E_F. We then systematically vary the coefficients to minimize the total least-squares error given by:

$$Error = \sum_{n=0}^{3}\left[\ln(G_{exp,n}) - \ln(G_{model,n})\right]^2 + \left[S_{exp,n} - S_{model,n}\right]^2$$

We use the natural logarithm of the conductance in determining the error so that we don't skew the fit towards higher conducting molecules or just the thermopower.

Model 1: A tight-binding model is constructed to represent the frontier orbital set that controls conductance in which a single energy level is assigned to each individual phenyl ring at an energy E_0. These are coupled to each other through a hopping parameter δ. The terminal phenyl states also interact with the electrodes through an imaginary energy independent self-energy term $-i\Gamma/2$. The Hamiltonian for this model is similar to that given in the main text, but without the gateway states. We solve for the transmission with the parameters that minimize the error between the model and experiment. As can be seen in Figure S9, this model gives a strictly linear increase in thermopower and underestimates the molecular conductance, and therefore does not fit the experimental data well.

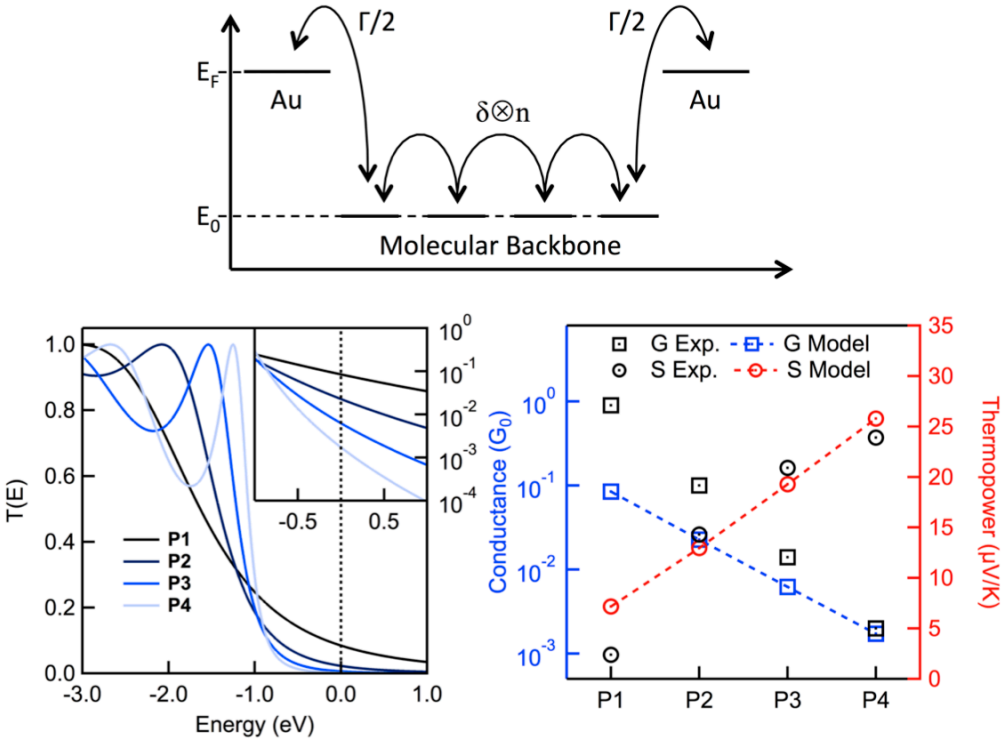

SI Figure S9: Transmission functions determined by solving the Hamiltonian that treats each individual phenyl as a separate state, but does not include the gateway state. The parameters used are: E_0 = -3.87, Γ = 2.74, δ = -1.6. A comparison of the model with experiment is also shown.

Model 2: This model introduces two gateway states at an energy ε that are tunnel coupled to each other through a length dependent parameter $\delta_n = \delta_0 e^{-\beta n/2}$. They also interact with the electrodes through an imaginary energy independent self-energy term $-i\Gamma/2$. The parameter β describes the long molecule limit of the decay of transmission. The Hamiltonian for this model is given below:

$$H = \begin{pmatrix} \varepsilon - i\Gamma/2 & \delta_n \\ \delta_n & \varepsilon - i\Gamma/2 \end{pmatrix}$$

The transmission function calculated from this Hamiltonian is:

$$\mathcal{T}_n(E) = \frac{\Gamma^2 \delta_n^2}{|(E - \varepsilon + i\Gamma/2)^2 - \delta_n^2|^2} \xrightarrow[\text{large } n]{} \frac{\Gamma^2 \delta_n^2}{((E-\varepsilon)^2 + \Gamma^2/4)^2}$$

The thermopower can then be calculated as usual. In the limit of large n, the approximate expression allows us to assess the impact of including an energy dependence in β:

$$S = -\frac{\pi^2 k_B^2 T}{3e} \frac{1}{T} \frac{dT}{dE} \xrightarrow[\text{large } n]{} \frac{-\pi^2 k_B^2 T}{3e} \left(\frac{(\varepsilon - E)}{4(\varepsilon - E)^2 + \Gamma^2} - n \frac{d\beta}{dE} \right)$$

Results from solving this Hamiltonian with the best-fit parameters are shown in Figure S10.

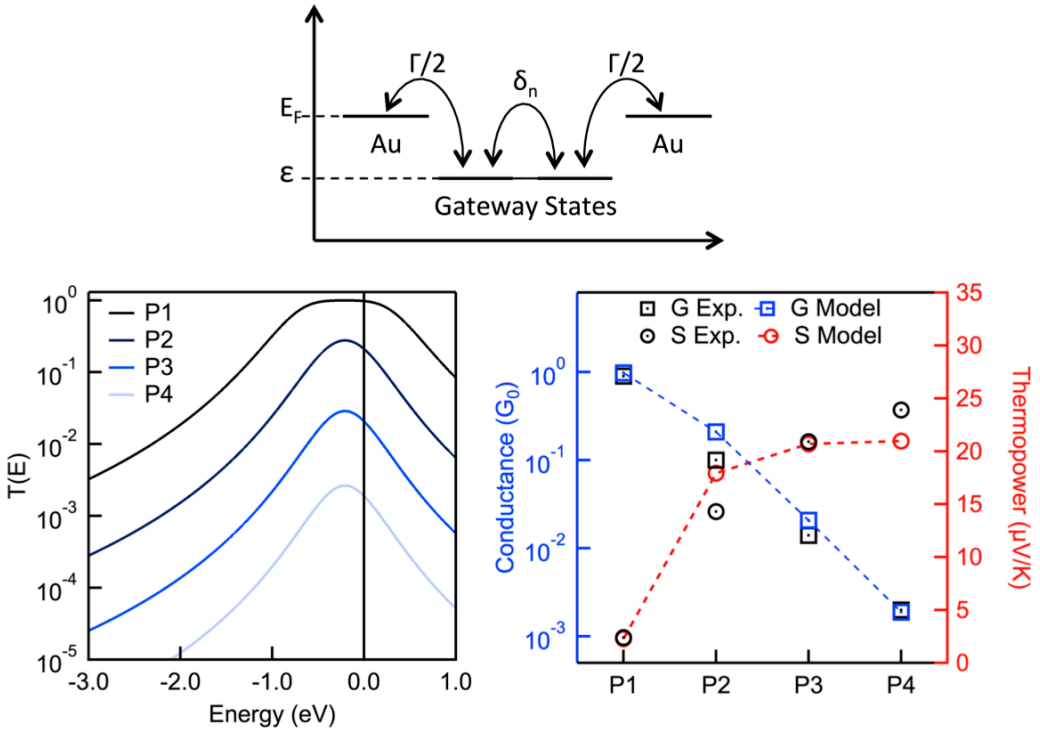

SI Figure S10: Transmission functions determined for all oligophenyls following the equations given with a constant β above using the parameters: ε = -0.21, Γ = 0.97, δ_0 = -0.45 and β = 2.4. A comparison of the model with experiment is shown in the bottom right panel.

Alkanes DFT Results Compared with Experiments:

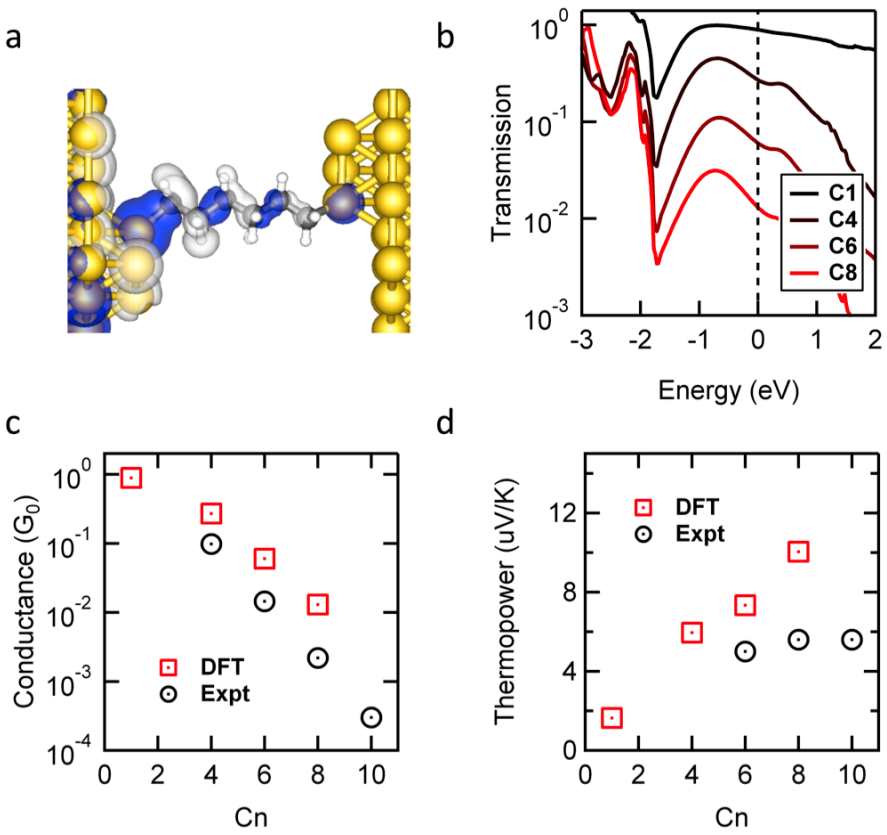

*Figure S11: (a) The optimized geometry of a **C6** junction with an isosurface plot of the scattering state at the Fermi energy. (b) Transmission curves calculated using DFT shown on a log scale for **C1**, **C4**, **C6**, and **C8**. (c) Conductance and (d) thermopower given as a function of molecular length for both experiment and DFT.*

References:

(1) Chen, W.; Widawsky, J. R.; Vázquez, H.; Schneebeli, S. T.; Hybertsen, M. S.; Breslow, R.; Venkataraman, L. *J. Am. Chem. Soc.,* **2011,** 133, (43), 17160-17163.

(2) Cheng, Z. L.; Skouta, R.; Vazquez, H.; Widawsky, J. R.; Schneebeli, S.; Chen, W.; Hybertsen, M. S.; Breslow, R.; Venkataraman, L. *Nat. Nano.,* **2011,** 6, (6), 353-357.

(3) Xu, B. Q.; Tao, N. J. *Science,* **2003,** 301, (5637), 1221-1223.

(4) Venkataraman, L.; Klare, J. E.; Nuckolls, C.; Hybertsen, M. S.; Steigerwald, M. L. *Nature,* **2006,** 442, (7105), 904-907.

(5) Widawsky, J. R.; Darancet, P.; Neaton, J. B.; Venkataraman, L. *Nano Lett.,* **2012,** 12, (1), 354-358.

(6) Malen, J. A.; Doak, P.; Baheti, K.; Tilley, T. D.; Segalman, R. A.; Majumdar, A. *Nano Lett.,* **2009,** 9, (3), 1164-1169.

(7) Datta, S., *Electronic Transport in Mesoscopic Systems*. Cambridge University Press: 1995.